# Classical Trajectory Calculations of Collision Energy Dependence of Partial Penning Ionization Cross Sections for $He^*(2^3S) + CH_3CN \rightarrow He + CH_3CN^+ + e^-$

**Tetsuji Ogawa and Koichi Ohno***

*Department of Chemistry, Graduate School of Science, Tohoku University, Aramaki Aoba-ku, Sendai 980-8578, Japan*

*Received: June 21, 1999; In Final Form: September 14, 1999*

Classical trajectory calculations are performed for the Penning ionization system $He^*(2^3S) + CH_3CN \rightarrow He(1^1S) + CH_3CN^+ + e^-$. Anisotropic model potentials of $He^*(2^3S) + CH_3CN$ are adopted to calculate the partial ionization cross sections for the ionic states, $\tilde{X}1^2E$, $\tilde{A}1^2A_1$, $\tilde{B}2^2E$, and $\tilde{C}2^2A_1$. Results of the calculations are compared with experimental collision energy dependence of partial ionization cross sections. Analyses of opacity functions indicate the attractive characteristics of the anisotropic interaction potential for the $\tilde{X}$ and $\tilde{A}$ states, the repulsive nature for the $\tilde{B}$ state, and the transition from the attractive to the repulsive features for the $\tilde{C}$ state.

## I. Introduction

In collisions of a molecule M with a metastable atom A* having excitation energy larger than the ionization potential of the molecule M, a chemi-ionization process known as Penning ionization ($A^* + M \rightarrow A + M^+ + e^-$)[1] can occur. One of the important variables in this process is the collision energy ($E_c$) between A* and M because collision energy dependence of the cross section reflects the shape of the interaction potential energy surface. Illenberger and Niehaus have shown that the collision energy dependence of the total ionization cross section $\sigma_T$ for atomic targets is mainly governed by the form of the entrance interaction potential.[2,3]

If several electronic states of the $M^+$ can be produced, $\sigma_T$ is the sum of the partial ionization cross sections $\sigma_i$ for all the states. The collision energy dependence of partial ionization cross sections has been measured for various molecular targets.[4−6] These measurements have revealed that $\sigma_i$ for the different final states may show different collision energy dependence reflecting the anisotropy of the interaction potential.

One of the examples is the system of $He^*(2^3S) + CH_3CN \rightarrow He + CH_3CN^+ + e^-$. Possible ionic states of $CH_3CN^+$ are the $\tilde{X}1^2E$, $\tilde{A}1^2A_1$, $\tilde{B}2^2E$, and $\tilde{C}2^2A_1$ states, which correspond to the removal of an electron from the $2e(\pi_{CN})$, $7a_1$ ($n_N$), $1e(\sigma_{CH})$, and $6a_1$ ($\sigma_{CC}$) molecular orbitals of $CH_3CN$, respectively.[7] In this system, observed collision energy dependence of the partial ionization cross section differs; $\sigma_{\tilde{X}}$ and $\sigma_{\tilde{A}}$ decrease with an increase of $E_c$, whereas $\sigma_{\tilde{B}}$ increases in the collision energy range of 70−350 meV.[6] These differences have been interpreted qualitatively in terms of the anisotropic interaction potential. A negative slope in a log $\sigma$−log $E_c$ plot could be connected to the long-range attractive part of the interaction potential, and a positive slope could be connected to the steepness of the repulsive part.[3] On the basis of the electron exchange mechanism of Penning ionization,[8] ionization should take place with high probability when the 1*s* orbital of a He atom overlaps effectively with the molecular orbital from which an electron is removed.[9] For example, ionization into the $\tilde{A}$ state, which corresponds to the removal of an electron from the nonbonding $n_N$ orbital, favorably occurs when a He* atom approaches the lone pair of the N atom. Thus, the collision energy dependence of $\sigma_{\tilde{A}}$ could be connected to the interaction potential around the N atom.

A theoretical treatment of Penning ionization can be divided into two steps on the basis of the Born−Oppenheimer separation of the electronic and nuclear motion. The first step is to calculate the potential energy surfaces. Because the entrance A*−M state can be considered as a resonance state, the potential energy for this state can be described in terms of local complex potential $V = V_0 - (i/2)\Gamma$; the real part $V_0$ governs the collision dynamics between A* and M, and the imaginary part $\Gamma$ is the ionization width for the decay of the A*−M state into the $A-M^+-e^-$ state. Hitherto, *ab initio* potential calculations for Penning systems have been limited to atomic targets and to a few molecular targets such as $He^*(2^3S)$−H,[10−15] $He^*$,[16,17] Li,[18,19] Na,[20−22] K,[23,24] $H_2$,[12,13,25] $N_2$,[26] and $H_2O$.[27,28] The second step is to calculate the collision dynamics on the local complex potential *V*. The collision process of Penning ionization for an atomic target has been discussed by Nakamura[29] and Miller.[30] Miller has derived formulas for a total ionization cross section in classical, semiclassical and quantum mechanical frameworks. Olson[31] has calculated collision energy dependencies of the total ionization cross section for $He^*(2^1S, 2^3S) + Ar$ using the classical formula of Miller; the $\Gamma$ used in the calculation is a semiempirical single-exponential form. The collision dynamics for the He*−$H_2$ system has been treated using the infinite order sudden (IOS),[12,32] close-coupling,[33,34] and classical trajectory[35−37] methods.

Recently, we have performed calculations of the partial ionization cross sections for the system of $He^*(2^3S) + N_2$ by the classical trajectory method based on simplified models for interaction potential and ionization width.[38] The partial ionization cross section for every ionic state monotonously increases with the increase in $E_c$, reflecting the repulsive characteristics of the interaction potential. The calculated collision energy dependence of the ionization cross section is in good agreement with the observation, much better than the calculation based on the *ab initio* potentials.[39]

In this study, the method used in our previous work is applied to the system of $He^*(2^3S) + CH_3CN$. The anisotropic nature of the collisional ionization dynamics is also discussed.

10.1021/jp992058+ CCC: $18.00 
Published on Web 11/10/1999

## II. Calculations

The method of the calculation used in this work has been reported in the previous paper.[38] It has been known that a metastable noble gas atom similarly behaves as an alkali-metal atom in interaction with another atom or molecule because of the outstanding importance of the outer electron as well as the irrelevance of the inner electrons. For example, the velocity dependence of the total scattering cross section of He*($2^3$S) by He, Ar, and Kr is similar to that of Li($2^2$S),[40] and the location of the well of the interaction potential and its depth are similar between He*($2^3$S) and Li($2^2$S) with various atomic targets.[5,41] Therefore, the interaction potential of the He*($2^3$S)−$CH_3CN$ system is expected to be very similar to that of the Li($2^2$S)−$CH_3CN$ system. The Li($2^2$S)−$CH_3CN$ potential calculated by the method given below is regarded as the real part of the local complex potential of He*($2^3$S)−$CH_3CN$ in the present study. *Ab initio* molecular orbital calculations[42] were performed to obtain the potential energy surface $V_0(R, \theta, \phi)$ of the Li($2^2$S)−$CH_3CN$ system, where $R$ is the distance between the Li (He*) atom and the center of mass of the $CH_3CN$ molecule, $\theta$ is the polar angle from the CCN axis of $CH_3CN$, and $\phi$ is the azimuthal angle. In these potential calculations, the structure of $CH_3CN$ was fixed at the experimental geometry. This is an approximation for the experimental condition where collisional processes occur relatively in a short time with respect to the molecular structural relaxation. The calculated equilibrium structure of $CH_3CNLi$ has been found to be only slightly deformed from a single $CH_3CN$ framework within ca. 0.01 Å.[6,43] Therefore, we believe that the effect of the molecular structural relaxation is not important. The basis set used is 6-31++G**. The second-order Møller−Plesset perturbation theory is used to include electron correlation effects. The full counterpoise method[44] was employed to correct the basis set superposition errors.

The ionization width $\Gamma^{(i)}$ of the entrance potential for each ionic state (denoted as $i$) is given by

$$\Gamma^{(i)} = 2\pi\rho^{(i)}|\langle\Phi_0|H^{el}|\Phi^{(i)}{}_{\epsilon}\rangle|^2 \quad (1)$$

where $H^{el}$ is the electronic Hamiltonian $\Phi_0$ and $\Phi^{(i)}{}_{\epsilon}$ are the electronic wavefunctions for the initial state (He*−$CH_3CN$) and the final state (He−$CH_3CN^+$ ($i$ th ionized state)−$e^-$), $\rho^{(i)}$ is the density of state, and $\epsilon$ indicates the kinetic energy of the ejected electron. The matrix element of eq 1 can be expanded in terms of two-electron integrals. The most important term in the case of He*($2^3$S) is

$$\langle\Phi_0|H^{el}|\Phi^{(i)}{}_{\epsilon}\rangle \approx -\left\langle\psi_{2s}(1)\phi_i(2)\left|\frac{1}{r_{12}}\right|\psi_{1s}(2)\phi_{\epsilon(i)}(1)\right\rangle \quad (2)$$

where $\psi_{2s}$ and $\phi_i$ are the orbitals for the initial state, the 2$s$ orbital of He and the $i$th orbital of the target molecule, respectively, and $\psi_{1s}$ and $\phi_{\epsilon(i)}$ are the orbitals for the final state, the 1s orbital of He and the continuum orbital of the ejected electron, respectively. This term can be approximated as

$$-C\langle\phi_i|\psi_{1s}\rangle\langle\psi_{2s}|\phi_{\epsilon(i)}\rangle \quad (3)$$

where the distance between the electrons is replaced by an average length to yield a constant factor of $C$. Such approximations have been widely used for semiempirical evaluation of the two-electron integrals related to charge transfer and electron exchange.[45] Because the 2s and continuum orbitals are too diffuse compared to the 1s and ionized orbitals, positional dependence of the ionization width is mainly governed by the more compact 1s and ionized orbitals. As long as the angular distribution of ejected electrons is neglected, the second overlap integral involving the continuum orbital has minor importance. Thus, the following formula can be used as the ionization width for the purpose of the present study:

$$\Gamma^{(i)} = K|\langle\phi_i|\psi_{1s}\rangle|^2 \quad (4)$$

where $K$ is a constant value. In this study, the $K$ value used is 14.6 eV, which was determined to reproduce the total ionization cross section for the case of He*($2^3$S)−$N_2$.[38] The orbital functions $\phi_i$ and $\psi_{1s}$ obtained from *ab initio* molecular orbital calculations with 6-31++G** basis functions for an isolated molecule ($CH_3CN$) and a helium atom, respectively, were used for the evaluation of the ionization width at each geometrical configuration.

In the present classical trajectory calculations, the geometry of the $CH_3CN$ molecule was fixed. The relative motion between the center of mass of the $CH_3CN$ molecule and the He* atom is governed by the equations of motion. The force acting on the He* atom is given by the gradient of the interaction potential,

$$\mathbf{F} = -\nabla V_0(R, \theta, \phi) \quad (5)$$

which depends on the relative distance ($R$) and the mutual orientation ($\theta$, $\phi$). The rotational motion of $CH_3CN$ was treated by using the quaternion parameters[38,46,47] in terms of the Euler angles. Once a set of the initial parameters of a trajectory have been determined, time evolution of these parameters is calculated to obtain the classical trajectory. The rate $W^{(i)}$ for ionization into each ionic state is given by

$$W^{(i)}(R, \theta, \phi) = \frac{\Gamma^{(i)}(R, \theta, \phi)}{\hbar} \quad (6)$$

To describe the dynamics of Penning ionization within a classical treatment, one should consider the survival factor, $S(t)$, which indicates the survival probability of He* in the excited state at a certain time $t$, as well as the ionization probability $P^{(i)}(t)$, which indicates the integrated probability that ionization into the $i$th ionic state has occurred before time $t$. These time-dependent quantities of $S(t)$ and $P^{(i)}(t)$ should satisfy the following differential equations:

$$\frac{dS(t)}{dt} = -S(t)\sum_i W^{(i)} \quad (7)$$

$$\frac{dP^{(i)}(t)}{dt} = S(t)W^{(i)} \quad (8)$$

From the initial conditions of $S(0) = 1$ and $P^{(i)}(0) = 0$, $S(t)$ and $P^{(i)}(t)$ are obtained by integrating the differential equations together with the trajectory calculation. $P^{(i)}(\infty)$ is the probability that ionization into the $i$th ionic state will occur during the whole span of the trajectory.

Initial conditions for numerous numbers of trajectories (10 000 trajectories for each collision energy) are generated as follows. The impact parameter $b$ is set to be $b = \xi b_{max}$, where $b_{max} = 9$ Å is the upper limit of $b$. Beyond this limit there are no effective trajectories leading to ionization. The parameter $\xi$ was treated as a random number between 0 and 1. The initial rotational energy for the $CH_3CN$ molecule was also obtained by a random generation technique so that the distribution obeys a Boltzmann distribution at 300 K to match the experimental condition, although the moment of inertia of $CH_3CN$ is not so

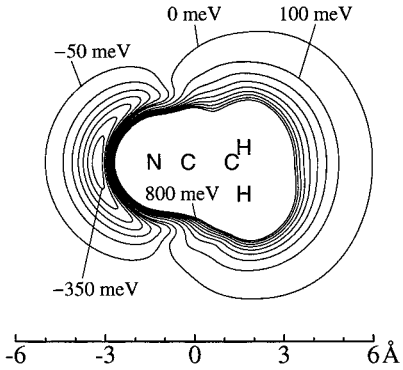


**Figure 1.** Contour map of the calculated interaction potential $V_0$. Energy spacing is 50 meV for $V_0 < 0$ and 100 meV for $V_0 > 0$.

small compared with that of $H_2O$ for which the effect of the initial rotational temperature is important.[48] A set of parameters including the orientation of the molecular axis and the rotational axis in addition to the impact parameter and the rotational energy was randomly generated to obtain initial conditions for a trajectory. The set of differential equations were numerically integrated by the fourth-order Runge−Kutta method with adaptive stepsize control.[49]

### III. Results and Discussion

Figure 1 shows the contour map of the calculated potential energy surface $V_0$ for Li($2^2$S)−$CH_3CN$, which we regard as the model for the real part of the potential of He*($2^3$S)−$CH_3CN$. The spacing of the contour lines is 50 meV for $V_0 < 0$ and 100 meV for $V_0 > 0$. The $V_0$ is attractive when a Li (He*) atom approaches the region around the N atom. The minimum of the potential is located on the coaxial line of the CN. The well depth is estimated to be about 380 meV. On the other hand, $V_0$ is repulsive around the methyl group, except for a shallow van der Waals well, whose depth is less than 10 meV. The intervals between the contour lines of the repulsive part of $V_0$ are very narrow around the nitrogen atom and are relatively wide around the methyl group.

Figure 2 shows the contour maps of the partial widths $\Gamma^{(i)}$ for ionization into the states correlating asymptotically to the $\tilde{X}$, $\tilde{A}$, $\tilde{B}$, and $\tilde{C}$ states of $CH_3CN^+$. The shapes in the contour maps reflect the electron distributions of the corresponding molecular orbitals: $2e(\pi_{CN})$, $7a_1(n_N)$, $1e(\sigma_{CH})$, and $6a_1(\sigma_{CC})$ orbitals, respectively. All $\Gamma^{(i)}$'s have the same symmetry as the corresponding molecular orbitals and decay exponentially as the distance between the He* and $CH_3CN$ increases. In Figure 2, the contour line of $V_0 = 100$ meV is also shown for reference. With the collision energy of 100 meV, He* hardly approaches within the contour line of $V_0 = 100$ meV. Therefore, the contour lines of $V_0$ indicate the boundaries to access for each collision energy. As seen from Figure 2, when a He* atom approaches the N atom along the CN axis, ionization into $\tilde{A}$ mainly occurs and ionization into $\tilde{X}$ and $\tilde{B}$ doesn't occur because of the vanishing $\Gamma^{(i)}$'s. When a He* atom approaches the N atom obliquely, ionization into $\tilde{X}$ should effectively occur. Ionization into $\tilde{B}$ should take place effectively when He* approaches the H atom. Ionization into $\tilde{C}$ takes place when He* approaches both sides of the CCN axis.

Figure 3 shows the calculated total ($\sigma_T$) and partial ($\sigma_{\tilde{X}}$, $\sigma_{\tilde{A}}$, $\sigma_{\tilde{B}}$, and $\sigma_{\tilde{C}}$) ionization cross sections as a function of the collision energy $E_c$. $\sigma_{\tilde{X}}$ and $\sigma_{\tilde{A}}$ decrease as the collision energy increases. $\sigma_{\tilde{A}}$ decreases more rapidly than $\sigma_{\tilde{X}}$. On the other hand, $\sigma_{\tilde{B}}$ increases as the collision energy increases. $\sigma_{\tilde{C}}$ decreases for $E_c < 100$ meV and increases for $E_c > 100$ meV. The gradients $m$ in the log $\sigma$ vs log $E_c$ plot are listed in Table 1 compared with experimental results.[6,50] In the measurement of Pasinszki et al.,[6] the collision energy dependences of $\sigma_{\tilde{X}}$ and $\sigma_{\tilde{A}}$ are negative and that of $\sigma_{\tilde{B}}$ is positive. The collision energy dependence of $\sigma_{\tilde{C}}$

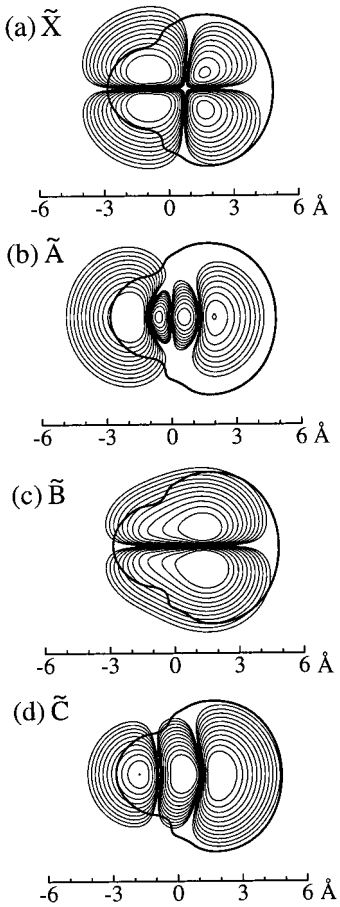


**Figure 2.** Contour maps of the calculated partial ionization widths $\Gamma^{(i)}$ for (a) $\tilde{X}$, (b) $\tilde{A}$, (c) $\tilde{B}$, and (d) $\tilde{C}$ states of $CH_3CN^+$. The values of contour lines are chosen to be $1 \times 2^{n-1}$ meV ($n = 1, 2, ..., 11$) for the $n$th line from the outside. The contour line of 100 meV of the real part potential $V_0$ is also shown by a thick line. The orientation of the $CH_3CN$ molecule is the same as that in Figure 1.

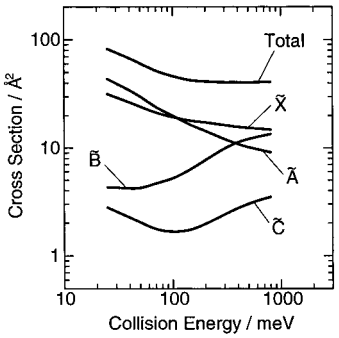


**Figure 3.** Collision energy dependence of the calculated total and partial ionization cross sections.

**TABLE 1: Gradients $m$ in log $\sigma$ vs log $E_c$ plot**

| ionic state | this work (70−400 meV) | experiment[a] (70−350 meV) | experiment (90−300 meV) |
|---|---|---|---|
| $\tilde{X}$ | −0.17 | −0.25 | −0.26 |
| $\tilde{A}$ | −0.45 | −0.40 | −0.47 |
| $\tilde{B}$ | 0.52 | 0.15 | 0.12 |
| $\tilde{C}$ | −0.44 (25−70 meV)<br>0.45 (140−400 meV) | | −0.18 |

[a] Pasinszki (ref 6). [b] Kishimoto (ref 50).

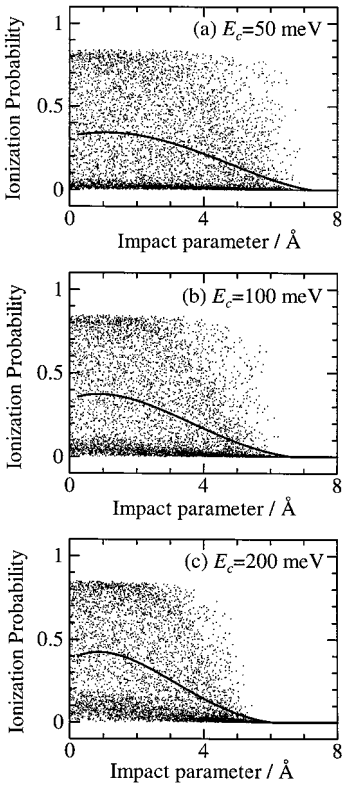


**Figure 4.** Ionization probabilities as functions of the impact parameter *b* (opacity functions) for ionization into the $\tilde{X}$ state of $CH_3CN^+$. From the top, $E_c = 50$ meV (a), 100 meV (b), and 200 meV (c), respectively. The average probability is shown by a solid curve.

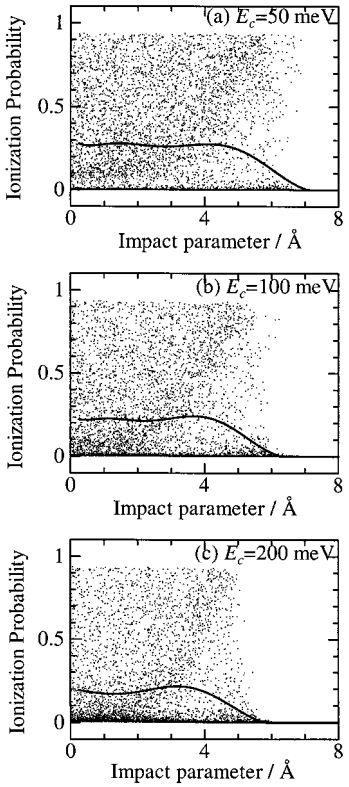


**Figure 5.** Ionization probabilities as functions of the impact parameter *b* (opacity functions) for ionization into the $\tilde{A}$ state of $CH_3CN^+$. From the top, $E_c = 50$ meV (a), 100 meV (b), and 200 meV (c), respectively. The average probability is shown by a solid curve.

was not obtained because the corresponding band intensity was very weak. Recently, Kishimoto et al. have measured the two-dimensional Penning ionization electron spectra (2D-PIES)[51,52] for this system.[50] The collision energy dependence of the partial ionization cross section derived from 2D-PIES is almost equal to that of Pasinszki for $\sigma_{\tilde{X}}$, $\sigma_{\tilde{A}}$, and $\sigma_{\tilde{B}}$. The collision energy dependence of $\sigma_{\tilde{C}}$ is found to be negative. However, the curve for $\sigma_{\tilde{C}}$ in the log $\sigma$ vs log $E_c$ plot is slightly bent and the slope seems to become positive at $E_c = 300$ meV. The collision energy dependence in this calculation agree qualitatively with experimental works; the relation of the gradients *m* for each ionic state is as $m_{\tilde{A}} < m_{\tilde{X}} < 0 < m_{\tilde{B}}$. Considering that the quantity used in this work is calculated by *ab initio* MO calculations except for the only one empirical parameter *K* in eq 4, these results are satisfactory.

The ionization cross section is the average of the ionization probabilities of many trajectories. We, then, examine each trajectory to obtain information about collisional dynamics. Figures 4−7 show ionization probabilities $P^{(i)}(\infty)$ into the $\tilde{X}$, $\tilde{A}$, $\tilde{B}$, and $\tilde{C}$ states of $CH_3CN^+$, respectively, for various trajectories. Because the target molecule is an anisotropic system, the ionization probability depends not only on the impact parameter *b* but also on the molecular orientation and the rotational motion. This is why many dots appear at a particular value of the impact parameter; many different situations are included for the same impact parameter value. As can be seen in Figures 4−7, Penning ionization probabilities are distributed between a certain upper bound and a lower one. The trajectories near the upper bound are most reactive, leading to ionization into the corresponding state, and those near the lower bound are least reactive. The sum of the partial ionization probabilities for each trajectory cannot exceed the unity. Therefore, because ionization probabilities for the $\tilde{A}$ state and the $\tilde{C}$ state are related

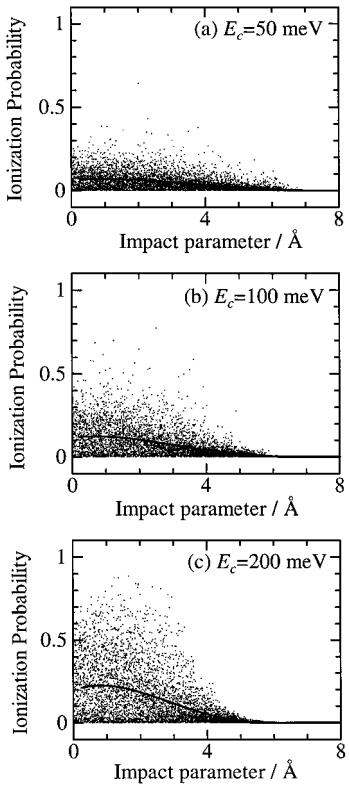


**Figure 6.** Ionization probabilities as functions of the impact parameter *b* (opacity functions) for ionization into the $\tilde{B}$ state of $CH_3CN^+$. From the top, $E_c = 50$ meV (a), 100 meV (b), and 200 meV (c), respectively. The average probability is shown by a solid curve.

to the electron distribution extending outside on the N end of the CN bond, their probabilities are limited to ca. 0.93 ($\tilde{A}$ state)

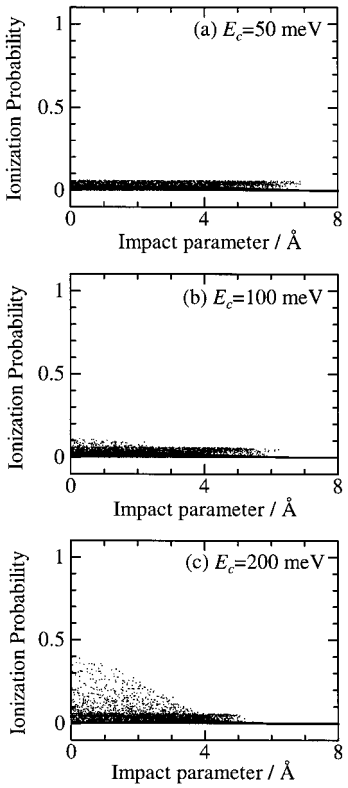


**Figure 7.** Ionization probabilities as functions of the impact parameter $b$ (opacity functions) for ionization into the $\tilde{C}$ state of $CH_3CN^+$. From the top, $E_c = 50$ meV (a), 100 meV (b), and 200 meV (c), respectively. The average probability is shown by a solid curve.

and ca. 0.06−0.07 ($\tilde{C}$ state). The sum of average partial probabilities shown by a solid curve in Figures 4−7 is also limited to less than the unity.

The opacity functions reflect the collision dynamics. Those for ionization in the $\tilde{X}$ and $\tilde{A}$ states have the following characteristics:

1. The upper boundary of the ionization probabilities are large and are almost independent of the impact parameter below the critical impact parameter $b_c$ (ca. 5−7 Å), whereas the ionization probabilities are almost 0 for the collision with the impact parameter larger than $b_c$.
2. The critical impact parameter $b_c$ becomes smaller as the collision energy increases; at $E_c = 50$ meV some trajectories with the impact parameter larger than 6 Å lead to ionization with high probability, but at $E_c = 200$ meV the trajectories with the impact parameter larger than 5.5 Å hardly lead to ionization.

These characteristics can be explained in terms of the theoretical treatment for a spherical attractive potential.[3] As the impact parameter $b$ is varied to larger values, the turning point, at which the distance between molecules is shortest, jumps at $b = b_c$. He* can approach a small distance for $b < b_c$ but rebounds outside the centrifugal barrier of the effective potential for $b > b_c$. For $b < b_c$ trajectories are mainly determined by the attractive forces and almost independent of $b$ and of $E_c$. As the collision energy increases, the $b_c$ decreases. The trajectories which lead to ionization into the $\tilde{X}$ and $\tilde{A}$ states with high probability are governed by the attractive potential around the nitrogen atom. The partial probability on the upper boundary is less than unity because the ionization into each ionic state is competitive.

Opacity functions for ionization into the $\tilde{B}$ state have the following characteristics.

1. The upper boundary of the ionization probabilities depends on the impact parameter. As the impact parameter changes to a smaller value, the ionization probability gradually increases.
2. The ionization probability increases as the collision energy increases for $b < 4$ Å.

These characteristics are typical for the repulsive potential such as $N_2$.[38] He* can approach smaller distances as the collision energy increases and as the impact parameter becomes smaller. The trajectories which lead to ionization into the $\tilde{B}$ state with high probability are governed by the repulsive part of the potential. In contrast, the ionization probability decreases as the collision energy increases for a larger impact parameter ($b > 4$ Å). This seems to be owing to the trajectories which are attracted by the potential around the nitrogen atom.

Opacity function for ionization into the $\tilde{C}$ state seems to be the overlap of that of the attractive and repulsive cases. This is interpreted as the fact that ionization into the $\tilde{C}$ state can take place both around the nitrogen atom and the C atom of the methyl group, as can be seen from $\Gamma^{(\tilde{C})}$ in Figure 2. For lower collision energy, ionization into the $\tilde{C}$ state takes place in the trajectories which approach the nitrogen atom, so the opacity function has the same characteristics as those of the $\tilde{A}$ state. In this case, the ionization cross section decreases as the collision energy increases. The sum of probability at the upper boundaries for the $\tilde{A}$ and $\tilde{C}$ states is almost unity, as mentioned above; the trajectories which give high probability to the $\tilde{A}$ state also give high probability to the $\tilde{C}$ state and give little probability to other states. For larger collision energy, ionization into the $\tilde{C}$ state takes place both at the N atom side and the opposite C atom side. As the collision energy increases, the ionization probability on the trajectories which approach the C atom of the methyl group increases. Therefore, the ionization cross section begins to increase at a certain collision energy of ca. 100 meV, as can be seen in Figure 3.

## IV. Conclusion

Classical trajectory calculations of the Penning ionization process based on the *ab initio* model potential and the overlap approximation for the ionization width are performed to obtain the collision energy dependence of the partial ionization cross sections. Calculated cross sections are compared with the experimental results. Although our calculations are a combination of the *ab initio* and semiempirical treatment, our results agree qualitatively with experimental results. Analyses of opacity functions indicate the attractive characteristics of the anisotropic interaction potential for the $\tilde{X}$ and $\tilde{A}$ states, the repulsive nature for the $\tilde{B}$ state, and the transition from the attractive to the repulsive features for the $\tilde{C}$ state. Investigation into the opacity functions leads to insight into the dynamics in the anisotropic potential energy surface.

## References and Notes

(1) Penning, F. M. *Naturwissenschaften* **1927**, *15*, 818.
(2) Illenberger, E.; Niehaus, A. *Z. Phys. B* **1975**, *20*, 33.
(3) Niehaus, A. *Adv. Chem. Phys.* **1981**, *45*, 399.
(4) Mitsuke, K.; Takami, T.; Ohno, K. *J. Chem. Phys.* **1989**, *91*, 1618.
(5) Ohno, K.; Takami, T.; Mitsuke, K.; Ishida, T. *J. Chem. Phys.* **1991**, *94*, 2675.
(6) Pasinszki, T.; Yamakado, H.; Ohno, K. *J. Phys. Chem.* **1995**, *99*, 14678.
(7) Kimura, K.; Katsumata, S.; Achiba, Y.; Yamazaki, T.; Iwata, S. *Handbook of HeI Photoelectron Spectra of Fundamental Organic Molecules*; Japan Scientific: Tokyo, 1981.
(8) Hotop, H.; Niehaus, A. *Z. Phys.* **1969**, *228*, 68.

(9) Ohno, K.; Mutoh, H.; Harada, Y. *J. Am. Chem. Soc.* **1983**, *105*, 4555.
(10) Miller, W. H.; Schaefer, H. F., III *J. Chem. Phys.* **1970**, *53*, 1421.
(11) Miller, W. H.; Slocomb, C. A.; Schaefer, H. F., III *J. Chem. Phys.* **1972**, *56*, 1347.
(12) Cohen, J. S.; Lane, N. F. *J. Chem. Phys.* **1977**, *66*, 586.
(13) Hickman, A. P.; Isaacson, A. D.; Miller, W. H. *J. Chem. Phys.* **1977**, *66*, 1483.
(14) Isaacson, A. D.; Miller, W. H. *Chem. Phys. Lett.* **1979**, *62*, 374.
(15) Movre, M.; Meyer, W. *J. Chem. Phys.* **1997**, *106*, 7139.
(16) Garrison, B. J.; Miller, W. H.; Schaefer, H. F. *J. Chem. Phys.* **1973**, *59*, 3193.
(17) Müller, M. W.; Bussert, W.; Ruf, M.-W.; Hotop, H.; Meyer, W. *Phys. Rev. Lett.* **1987**, *59*, 2279.
(18) Merz, A.; Müller, M. W.; Ruf, M.-W.; Hotop, H.; Meyer, W.; Movre, M. *Chem. Phys. Lett.* **1989**, *160*, 377.
(19) Kimura, M.; Lane, N. F. *Phys. Rev. A* **1990**, *41*, 5938.
(20) Cohen, J. S.; Martin, R. L.; Lane, N. F. *Phys. Rev. A* **1985**, *31*, 152.
(21) Padial, N. T.; Cohen, J. S.; Martin, R. L.; Lane, N. F. *Phys. Rev. A* **1989**, *40*, 117.
(22) Merz, A.; Müller, M. W.; Ruf, M.-W.; Hotop, H.; Meyer, W.; Movre, M. *Chem. Phys.* **1990**, *145*, 219.
(23) Padial, N. T.; Martin, R. L.; Cohen, J. S.; Lane, N. F. *Phys. Rev. A* **1989**, *39*, 2715.
(24) Scheibner, K. F.; Cohen, J. S.; Martin, R. L.; Lane, N. F. *Phys. Rev. A* **1987**, *36*, 2633.
(25) Isaacson, A. D.; Hickman, A. P.; Miller, W. H. *J. Chem. Phys.* **1977**, *67*, 370.
(26) Ishida, T. *Chem. Phys. Lett.* **1992**, *191*, 1.
(27) Haug, B.; Morgner, H.; Staemmler, V. *J. Phys. B* **1985**, *18*, 259.
(28) Ishida, T. *J. Chem. Phys.* **1995**, *102*, 4169.
(29) Nakamura, H. *J. Phys. Soc. Jpn.* **1969**, *26*, 1473.
(30) Miller, W. H. *J. Chem. Phys.* **1970**, *52*, 3563.
(31) Olson, R. E. *Phys. Rev. A* **1972**, *6*, 1031.
(32) Martin, D. W.; Siska, P. E. *J. Chem. Phys.* **1985**, *82*, 2630.
(33) Hickman, A. P.; Isaacson, A. D.; Miller, W. H. *J. Chem. Phys.* **1977**, *66*, 1492.
(34) Martin, D. W.; Siska, P. E. *J. Chem. Phys.* **1988**, *89*, 240.
(35) Preston, R. K.; Cohen, J. S. *J. Chem. Phys.* **1976**, *65*, 1589.
(36) Vojtík, J. *Chem. Phys.* **1996**, *209*, 367.
(37) Vojtík, J.; Kotal, R. *Chem. Phys. Lett.* **1996**, *255*, 251.
(38) Ogawa, T.; Ohno, K. *J. Chem. Phys.* **1999**, *110*, 3773.
(39) Ishida, T.; Horime, K. *J. Chem. Phys.* **1996**, *105*, 5380.
(40) Rothe, E. W.; Neynaber, R. H.; Trujillo, S. *J. Chem. Phys.* **1965**, *42*, 3310.
(41) Hotop, H. *Radiat. Res.* **1974**, *59*, 379.
(42) Frisch, M. J.; Trucks, G. W.; Schlegel, H. B.; Gill, P. M. W.; Johnson, B. G.; Robb, M. A.; Cheeseman, J. R.; Keith, T.; Petersson, G. A.; Montgomery, J. A.; Raghavachari, K.; Al-Laham, M. A.; Zakrzewski, V. G.; Ortiz, J. V.; Foresman, J. B.; Cioslowski, J.; Stefanov, B. B.; Nanayakkara, A.; Challacombe, M.; Peng, C. Y.; Ayala, P. Y.; Chen, W.; Wong, M. W.; Andres, J. L.; Replogle, E. S.; Gomperts, R.; Martin, R. L.; Fox, D. J.; Binkley, J. S.; Defrees, D. J.; Baker, J.; Stewart, J. P.; Head-Gordon, M.; Gonzalez, C.; Pople, J. A. *Gaussian 94*, Revision C.3; Gaussian, Inc.: Pittsburgh, PA, 1995.
(43) Ohshimo, K.; Tsunoyama, H.; Yamakita, Y.; Misaizu, F.; Ohno, K. *Chem. Phys. Lett.* **1999**, *301*, 356.
(44) Boys, S. F.; Bernardi, F. *Mol. Phys.* **1970**, *19*, 553.
(45) Miller, W. H.; Morgner, H. *J. Chem. Phys.* **1977**, *67*, 4923.
(46) Evans, D. J. *Mol. Phys.* **1977**, *34*, 317.
(47) Evans, D. J.; Murad, S. *Mol. Phys.* **1977**, *34*, 327.
(48) Ishida, T. *J. Chem. Phys.* **1996**, *105*, 1392.
(49) Press, W. H.; Teukolsky, S. A.; Vetterling, W. T.; Flannery, B. P. *NUMERICAL RECIPES in C*; Cambridge University Press: Cambridge, 1988.
(50) Kishimoto, N.; Pasinszki, T.; Ohno, K. Unpublished work.
(51) Ohno, K.; Yamakado, H.; Ogawa, T.; Yamata, T. *J. Chem. Phys.* **1996**, *105*, 7536.
(52) Kishimoto, N.; Aizawa, J.; Yamakado, H.; Ohno, K. *J. Phys. Chem. A* **1997**, *101*, 5038.